PHYSICAL REVIEW A **83**, 063816 (2011)

Dark-bright gap solitons in coupled-mode one-dimensional saturable waveguide arrays

Rong Dong, Christian E. Rüter, and Detlef Kip
Faculty of Electrical Engineering, Helmut Schmidt University, D-22043 Hamburg, Germany

Jesús Cuevas
Grupo de Física No Lineal, Departamento de Física Aplicada I, Escuela Politécnica Superior, C/ Virgen de África, 7, E-41011 Sevilla, Spain

Panayotis G. Kevrekidis
Department of Mathematics and Statistics, University of Massachusetts, Amherst, Massachusetts 01003-4515, USA

Daohong Song and Jingjun Xu
Key Laboratory of Weak-Light Nonlinear Photonics, Ministry of Education and TEDA, Applied Physics School, Nankai University, Tianjin 300457, China

(Received 13 April 2011; published 15 June 2011)

In the present work, we consider the dynamics of dark solitons as one mode of a defocusing photorefractive lattice coupled with bright solitons as a second mode of the lattice. Our investigation is motivated by an experiment that illustrates that such coupled states can exist with both components in the first gap of the linear band spectrum. This finding is further extended by the examination of different possibilities from a theoretical perspective, such as symbiotic ones where the bright component is supported by states of the dark component in the first or second gap, or nonsymbiotic ones where the bright soliton is also a first-gap state coupled to a first or second gap state of the dark component. While the obtained states are generally unstable, these instabilities typically bear fairly small growth rates, which enable their observation for experimentally relevant propagation distances.

DOI: 10.1103/PhysRevA.83.063816 PACS number(s): 42.65.Tg, 05.45.Yv, 42.82.Et, 63.20.Pw

I. INTRODUCTION

The examination of the Hamiltonian continuum model with periodic potentials and its discrete analog of lattice dynamical systems has been a topic of increasing popularity over the last few years [1]. This is mainly due to their wide applicability in diverse physical contexts including, but not limited to, the spatial dynamics of optical beams in coupled waveguide arrays [2], optically induced photonic lattices in nonlinear optics [3], temporal evolution of Bose-Einstein condensates (BECs) in optical lattices in soft-condensed matter physics [4], and the DNA double strand in biophysics [5].

A principal research theme in this direction is the study of existence and stability of coherent structures in these models and their feasibility in experiments. Several years ago, fabrication of nonlinear optical AlGaAs waveguide arrays [6] provided a first prototype through which many initial investigations arose, such as discrete diffraction, Peierls barriers, diffraction management [7], and gap solitons [8]. So far numerous fundamental investigations have been pursued in waveguide arrays, including modulational instability [9] and four-wave-mixing effects arising from the coupling of multiple components [10], as well as the study of interactions of solitary waves with surfaces [11]. Subsequently the formation of optically induced photonic lattices in photorefractive crystals became an ideal platform for the observation of various types of solitonic structures. The theoretical proposal [12] and rapid experimental realization of such (mainly two-dimensional) lattices [13,14] enabled the observation of, among other things, dipole [15], necklace [16], and rotary [17] solitons as well as discrete [18,19] and gap [20] vortices. Recently waveguide arrays in lithium niobate ($LiNbO_3$) crystal, which possess a self-defocusing nonlinearity, have found significant applications in the study of modulation instability [21], beam interactions [22], dark discrete solitons [23], bright gap solitons [24], and dark solitons in higher gaps [25], as well as Rabi oscillations [26].

Our goal in this work is to consider the case of vector solitons. Although they have been studied both in the focusing case of bright-vector solitons in strontium barium niobate [27] and in the defocusing case of bright-gap-vector solitons in $LiNbO_3$ [28], much less work has been done in multicomponent settings. Instead of mixtures of two solitary waves of the same type as in the above cases, we aim to examine the mixture of a bright with a dark soliton in photorefractive defocusing waveguide arrays. Such dark-bright states were first created in the absence of lattices in photorefractive crystals more than a decade ago [29], and their interactions were partially monitored [30]. In the context of BECs such solitary waves were also predicted theoretically [31], and generalizations thereof were considered as well (such as the dark-dark-bright or bright-bright-dark spinor variants of Ref. [32]). However, it was only quite recently that such structures were experimentally observed [33–36]. This has led to a renewed interest in this theme, by addressing the interactions of dark-bright solitons from an integrable theory [37] or numerical [38] perspective, as well as their higher-dimensional generalizations [39]. To the best of our knowledge, there is no earlier investigation of such states in models with a periodic potential except in the context of nonlinear dynamical lattices [40].

Our motivation, presented in Sec. II, stems from an experiment in defocusing $LiNbO_3$ waveguide arrays where a dark soliton state in the first gap (we will refer to this type of state as a "bubble" in this paper) is coupled to a bright soliton

in the same gap. We will show that these two waveforms coexist as a solitonic entity. Also, we will present conditions under which such a molecule may break up in its constituents. This, in turn, motivates a more detailed theoretical study of the different types of dark-bright states that can exist in the system. Such coupled states will be identified between either a bubble (in the first gap) or a higher-gap (i.e., the second gap in this case) dark soliton in the one component with either a regular bright soliton or a bright gap soliton. When a bubble or dark soliton couples to a regular bright one, we refer to these solitons as symbiotic because the bright component cannot exist without the supporting dark component (due to the defocusing nature of the nonlinearity). For the coupling with a bright-gap soliton, because both components can persist individually, we refer to these states as nonsymbiotic. We find such multicomponent solitary waves to be only weakly unstable, which is consonant with our ability to experimentally observe case examples of such states. In Sec. III, we set up the model problem and benchmark it against experimental data by identifying its linear band spectrum. In Sec. IV the numerical results for the above soliton families will be given. Finally, in Sec. V we summarize our findings and present conclusions as well as relevant directions for future study.

II. EXPERIMENTAL MOTIVATION

To experimentally investigate such molecular solitonic states of dark and bright solitons, we used a one-dimensional waveguide array (WA) fabricated on an iron-doped lithium niobate ($LiNbO_3$) substrate by in-diffusion of titanium at high temperature. Arising from the bulk photovoltaic effect, the substrate crystal displays a saturable type of defocusing nonlinearity [41]. The transverse direction z is parallel to the ferroelectric c axis. The direction of light propagation is along the y axis. The array investigated in the following experiments consists of 250 channels and has a grating period $\Lambda = 8.5\ \mu$m, which is the summation of the channel width of 5 μm and a spacing of 3.5 μm between adjacent channels. One of the end facets of the waveguide array sample is polished to optical quality to allow for direct observation of the out-coupled light from the array with the help of a CCD camera.

In our experimental setup, we employed the prism-coupler scheme, with which we can selectively excite different Bloch modes in any desired band. Furthermore, with this method we can determine accurately the band structure of the waveguide array [42]. The experimental layout is sketched in Fig. 1. First, the input light with a wavelength of 532 nm from a frequency-doubled Nd:YVO_4 laser is expanded by a beam expander into a plane wave and then split into two separate beams. One beam propagates through a phase mask covering half of the beam along the transverse direction z. As a consequence, the covered half of the input beam experiences an additional π phase shift, and thus a dark notch is generated at the center of the intensity profile. Another beam is modulated by an oscillating mirror driven by a function generator. With applied external modulation, this beam is mutually incoherent with respect to the other beam: Since the phase modulation is much faster than the build-up time of the nonlinearity of our photorefractive crystal, no stationary interference pattern forms with the other beam. With the combination of two

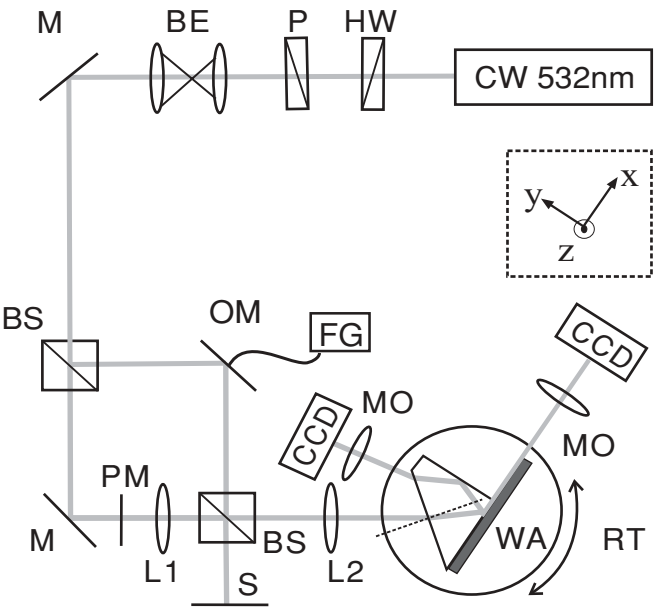

FIG. 1. Schematic experimental setup: HW, half-wave plate; P, polarizer; BE, beam expander; Ms, mirrors; BSs, beam splitters; OM, oscillating mirror; FG, function generator; PM, phase mask; S, screen; L1 and L2, cylindrical lenses; MOs, microscopic objectives; CCDs, CCD cameras; PD, photodiode; WA, waveguide array.

cylindrical lenses L1 and L2, the beam passing the phase mask is then imaged onto the waveguide. Here the focal lengths of the two lenses are chosen in order to generate an ideal width of the dark notch covering about two channels, which is the input light pattern for the excitation of a dark soliton. The other beam is focused meanwhile by lens L2 with a diameter of roughly 10 μm and serves as the excitation light for the bright soliton. Both beams are coupled into the waveguide array and copropagate until they reach the end facet of the sample. With a high-resolution CCD camera, in combination with a 20× microscopic objective lens, we can monitor around 25 channels of the intensity distribution on the end facet. With this setup, it is possible to adjust the input light distribution for both, the bright soliton and the dark soliton separately, for example, the relative locations of the two solitons on the waveguide array as well as different excitation angles for modes originating from different bands.

In the experiment, a bright gap soliton was excited from the first and a dark soliton from the second band (a "bubble" according to our notation above), both at the edge of the Brillouin zone. The centers of both solitons were carefully adjusted to overlap on the same waveguide channel. We first checked under low optical power (less than 2 nW per channel) the linear diffraction behavior of both the dark component [Fig. 2(a), top row] and bright component [Fig. 2(a), bottom row]. Then, by blocking one of the input beams, we formed individual gap solitons (either dark or bright) by increasing the optical power to appropriately high values [Fig. 2(b)]. In all nonlinear experiments, the dark soliton from the second band was formed under 150 nW optical power per channel. In order to analyze the existence interval of the bubble-bright composite solitons, the input light power of the bright soliton was varied, resulting in different power ratios of dark and bright

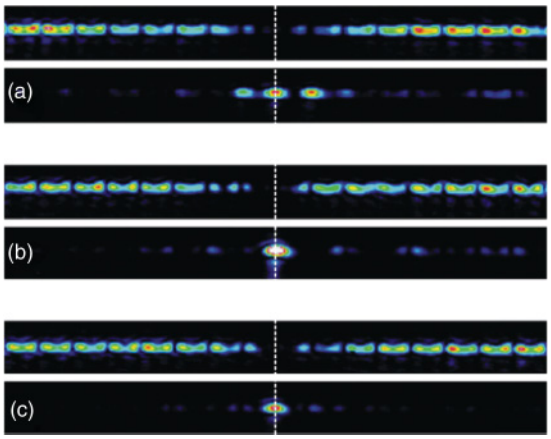

FIG. 2. (Color online) Experimental results of light intensity distribution on the output facet showing linear diffraction (a) and soliton formation of individual bright and dark components (b). When both beams are launched with a power ratio of 4:3, a robust bubble-bright soliton is formed (c) where both bright and dark components are centered on the same channel.

components. At first, a bright soliton was formed at 200 nW per channel, yielding a power ratio to the bright and dark solitons of 4:3. In this case we observe a robust coexistence of the two components at the output facet, as shown in Fig. 2(c).

However, when we excite the bright soliton at much higher power (400 nW per channel, resulting in a power ratio of 8:3), the propagation constant μ_b of the bright component in this scenario is further decreased below the existence threshold (see also the theoretical analysis below), while the propagation constant μ_d of the dark component's bubble state remains essentially unaffected. The result of the experiment in this situation is a clear spatial shift of the bubble center by one waveguide channel [Fig. 3(a)] due to the coupling with the bright soliton. This shift may be understood as the initial phase

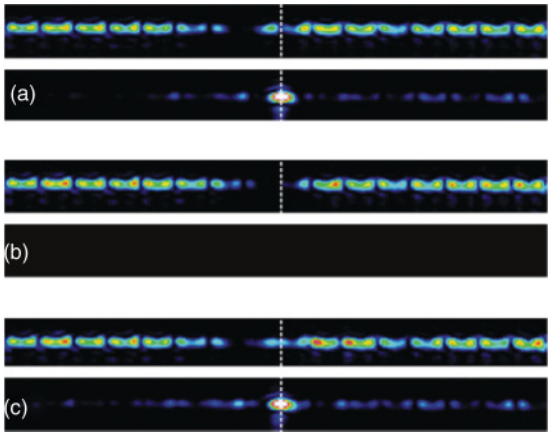

FIG. 3. (Color online) When the input power ratio is increased (dominating bright component) a shift of the dark soliton center is experimentally observed (a). A restoration of the center position of the bubble state appears when the bright component is blocked (b). This process is reversible in the experiment, and the bubble is forced to shift again from the center position when the bright beam is switched on again (c).

of a repulsive interaction of the two constituents and thus suggests the nonexistence (or strong instability) of bubble-bright solitons for these input conditions. After reaching the steady state for the input power ratio 8:3, we blocked the input beam used for excitation of the bright soliton. Because the nonlinearity in lithium niobate is noninstantaneous, the negative defect formed by the bright beam is still present and is only slowly erased due to the photoconductivity generated by the remaining dark beam. As a consequence, in the μ_d-μ_b plane (see the left panel in Fig. 6) we now move upward (i.e., μ_b increases) on a vertical line, reaching back to the existence regime of robust bubble solitary waves. We thus observe a reversible effect, presented in Fig. 3(b): After the bright soliton is blocked, the dark soliton is restored to its original location. This restoration proves directly the repulsive influence from the dominant bright soliton. When the bright component is switched on again in Fig. 3(c), once again the strong repulsion between bright and dark components forces the dark soliton to be shifted by one channel.

III. MODEL SETUP

In the following discussion, we will consider composite solitons with a dark (or bubble) wave in one component coupled with a bright mode in the second component in the context of TE-TE modes for the geometry of our waveguide array. We start by presenting the underlying model in the full dimensional form with the paraxial approximation, and then we discuss the nondimensional variant of the model, which will be used for our numerical computations.

A. Dynamical equations

The paraxial equations for coupled TE-TE modes of the two beams represented by E_d and E_b in this discussion are given by

$$\begin{aligned} &i\partial_X E_d + \frac{1}{2k}\partial_{ZZ} E_d \\ &\quad + \frac{k}{n_s}\left[\Delta n(Z) + \Delta n_{nl}\frac{|E_d|^2 + |E_b|^2}{1 + |E_d|^2 + |E_b|^2}\right] E_d = 0, \\ &i\partial_X E_b + \frac{1}{2k}\partial_{ZZ} E_b \\ &\quad + \frac{k}{n_s}\left[\Delta n(Z) + \Delta n_{nl}\frac{|E_d|^2 + |E_b|^2}{1 + |E_d|^2 + |E_b|^2}\right] E_b = 0, \end{aligned} \tag{1}$$

with $\Delta n(Z)$ the refractive index profile and the propagation direction denoted as the x direction. One can find "stationary" solutions of this system by defining

$$E_d(X,Z) = e^{i\beta_d X} u(Z), \qquad E_b(X,Z) = e^{i\beta_b X} v(Z), \tag{2}$$

where $\beta_{d,b}$ are the propagation constants in the X direction and $u(Z)$ and $v(Z)$ the amplitude profiles of each TE mode, which, in turn, satisfy

$$\begin{aligned} &-\beta_d u + \frac{1}{2k}\partial_{ZZ} u + \frac{k}{n_s}\left[\Delta n(Z) + \Delta n_{nl}\frac{u^2 + v^2}{1 + u^2 + v^2}\right] u = 0, \\ &-\beta_b v + \frac{1}{2k}\partial_{ZZ} v + \frac{k}{n_s}\left[\Delta n(Z) + \Delta n_{nl}\frac{u^2 + v^2}{1 + u^2 + v^2}\right] v = 0, \end{aligned} \tag{3}$$

The values used in the experiments are the following:

$$n_s = 2.2341, \quad \lambda = 532\ \text{nm}, \quad \Lambda = 8.5\ \mu\text{m},$$
$$k = \frac{2\pi n_s}{\lambda} = 26.386\ \mu\text{m}^{-1}, \quad \Delta n_{nl} = 2.5 \times 10^{-4} \tag{4}$$

(cf. also the discussion given in Sec. II) where n_s is the refractive index of the $LiNbO_3$ substrate for extraordinary polarized light, λ is the wavelength of the input light, Λ is the period of the waveguide array, and Δn_{nl} is the maximum refractive index change induced by the nonlinearity.

The refractive index profile can be determined by adjusting the experimental Bloch bands showing the change of the effective refractive index $\Delta n_{\text{eff}} \equiv n_{\text{eff}} - n_s$, with $n_{\text{eff}} = \beta k_0$ and $k_0 = k/n_s$ being the transverse wave vector in vacuum. The refractive index is then given by

$$\Delta n(Z) = \Delta n_0 + \Delta n_1 V(Z) \tag{5}$$

with

$$V(Z) = \cos\left(\frac{2\pi Z}{\Lambda}\right) - 0.25\cos\left(\frac{4\pi Z}{\Lambda}\right) \tag{6}$$

and

$$\Delta n_0 - n_s = 27.567 \times 10^{-4}, \quad \Delta n_1 = 8.35 \times 10^{-4}. \tag{7}$$

Figure 4 shows the correspondence between the experimentally observed Bloch bands [42] and the theoretically computed ones. Clearly the above set of parameters offers a very good handle on the linear part of the problem.

B. Nondimensional equations and parameters

The nondimensional version of the system of Eqs. (1) is given by

$$i\partial_x u + \frac{1}{2}\partial_{zz}u + [\eta^0 + \eta V(z)]u + \nu\frac{u^2+v^2}{1+u^2+v^2}u = 0,$$
$$i\partial_x v + \frac{1}{2}\partial_{zz}v + [\eta^0 + \eta V(z)]v + \nu\frac{u^2+v^2}{1+u^2+v^2}v = 0, \tag{8}$$

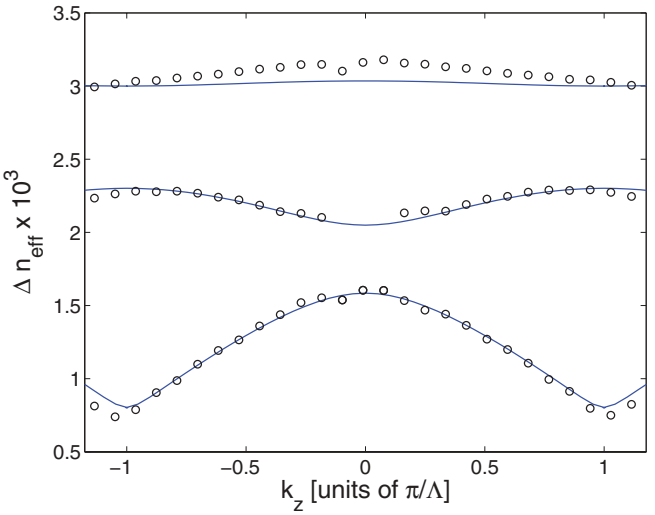

FIG. 4. (Color online) Bloch bands numerically (full lines) and experimentally (circles) determined.

while the stationary states are solutions of

$$-\mu_d u + \frac{1}{2}\partial_{zz}u + [\eta^0 + \eta V(z)]u + \nu\frac{u^2+v^2}{1+u^2+v^2}u = 0,$$
$$-\mu_b v + \frac{1}{2}\partial_{zz}v + [\eta^0 + \eta V(z)]v + \nu\frac{u^2+v^2}{1+u^2+v^2}v = 0. \tag{9}$$

The nondimensional parameters are related to the experimental ones by the following relations:

$$\mu_{d,b} = \frac{k\Lambda^2\beta_{d,b}}{\alpha^2}, \qquad \nu = \pm\frac{k^2\Lambda^2\Delta n_{nl}}{\alpha^2 n_s}, \tag{10}$$

$$\eta = \frac{k^2\Lambda^2\Delta n_1}{\alpha^2 n_s}, \qquad \eta^0 = \frac{k^2\Lambda^2\Delta n_0}{\alpha^2 n_s}. \tag{11}$$

The parameter α has been introduced so that the nondimensional values are of $O(1)$. Throughout the calculations, it has been fixed to $\alpha = 10$. The sign of ν indicates either self-focusing (positive) or self-defocusing (negative). Additionally, the nondimensional distances are given by

$$z = \alpha Z/\Lambda, \qquad x = \frac{\beta_{d,b}}{\mu_{d,b}}X = \frac{\alpha^2}{k\Lambda^2}X. \tag{12}$$

The refractive index profile and parameters are given now by

$$V(z) = \cos\left(\frac{2\pi z}{\alpha}\right) - 0.25\cos\left(\frac{4\pi z}{\alpha}\right), \tag{13}$$

$$\eta = 0.1880, \qquad \eta^0 = 0.6207, \qquad \nu = \pm 0.0563, \tag{14}$$

and the change of the effective refractive index is

$$\Delta n_{\text{eff}} = \frac{\beta_{d,b}\lambda}{2\pi} = \frac{\alpha^2\lambda^2\mu_{d,b}}{4\pi^2 n_s\Lambda^2} \tag{15}$$

for each (dark and bright) component.

C. Stability equations

Once stationary solutions of the boundary value problem (with periodic or antiperiodic boundary conditions, depending on the nature of the examined solution) of Eqs. (9) are identified, their linear stability is considered by means of a Bogolyubov-de Gennes analysis. Namely, small perturbations [of order $O(\delta)$, with $0 < \delta \ll 1$] are introduced in the form

$$E_d(z,x) = e^{i\mu_d x}\{u_0(z) + \delta[P(z)e^{i\omega z} + Q^*(z)e^{-i\omega^* z}]\},$$
$$E_b(z,x) = e^{i\mu_b x}\{v_0(z) + \delta[R(z)e^{i\omega z} + S^*(z)e^{-i\omega^* z}]\}, \tag{16}$$

and the ensuing linearized equation are then solved to $O(\delta)$, leading to the following eigenvalue problem:

$$\omega\begin{pmatrix} P(z) \\ Q(z) \\ R(z) \\ S(z) \end{pmatrix} = \begin{pmatrix} L_1 & L_2 & L_3 & L_3 \\ -L_2 & -L_1 & -L_3 & -L_3 \\ L_3 & L_3 & L_4 & L_5 \\ -L_3 & -L_3 & -L_5 & -L_4 \end{pmatrix}\begin{pmatrix} P(z) \\ Q(z) \\ R(z) \\ S(z) \end{pmatrix}, \tag{17}$$

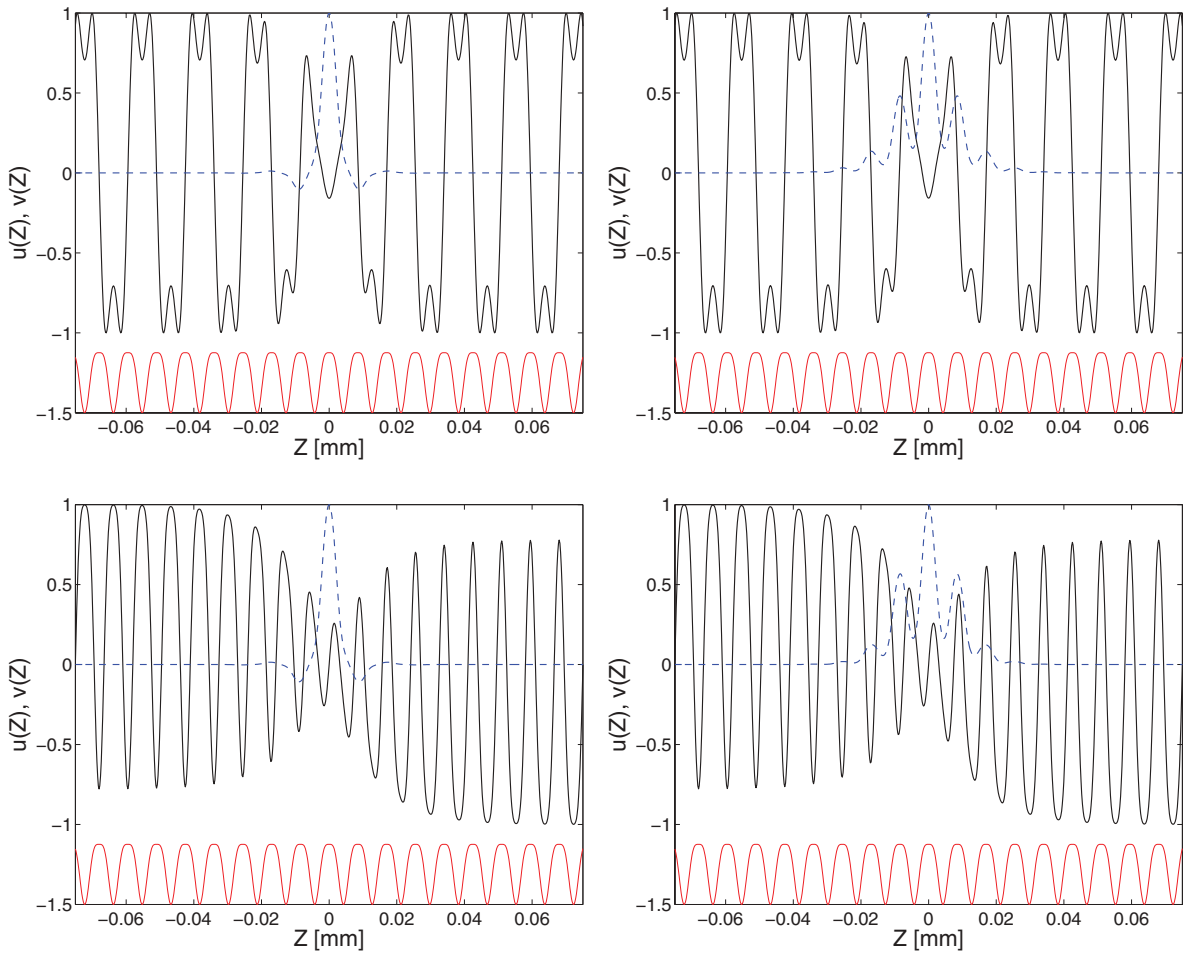

FIG. 5. (Color online) Soliton profiles for bubble-bright (top panels) and dark-bright (bottom panels) solitons. Profile of the electric field for a NS-BBS with $\mu_b = 0.64$ and $\mu_d = 0.49$ (left panel in top line), S-BBS with $\mu_b = 0.66$ and $\mu_d = 0.48$ (right panel in top line), NS-DBS with $\mu_b = 0.65$ and $\mu_d = 0.33$ (left panel in bottom line), and S-DBS with $\mu_b = 0.67$ and $\mu_d = 0.32$ (right panel in bottom line). Blue dashed lines: input field of the bright component. Black solid lines: input field of the dark component. The red solid lines in each case illustrate a rescaled form of $V(x)$ to indicate the location of the potential wells.

for the eigenfrequency ω and the associated eigenvector $(P(z), Q(z), R(z), S(z))^T$, where L_j, $j = 1 \ldots 5$ are the following operators:

$$
\begin{aligned}
L_1 &= -\mu_d + \frac{1}{2}\frac{d^2}{dz^2} + [\eta^0 + \eta V(z)] \\
&\quad + \nu\left[\frac{u_0^2 + v_0^2}{1 + u_0^2 + v_0^2} + \frac{u_0^2}{\left(1 + u_0^2 + v_0^2\right)^2}\right], \\
L_2 &= \nu\frac{u_0^2}{\left(1 + u_0^2 + v_0^2\right)^2}, \\
L_3 &= \nu\frac{u_0 v_0}{\left(1 + u_0^2 + v_0^2\right)^2}, \\
L_4 &= -\mu_b + \frac{1}{2}\frac{d^2}{dz^2} + [\eta^0 + \eta V(z)] \\
&\quad + \nu\left[\frac{u_0^2 + v_0^2}{1 + u_0^2 + v_0^2} + \frac{v_0^2}{\left(1 + u_0^2 + v_0^2\right)^2}\right], \\
L_5 &= \nu\frac{v_0^2}{\left(1 + u_0^2 + v_0^2\right)^2},
\end{aligned}
\tag{18}
$$

where it has been taken into account that $u_0(z), v_0(z) \in \mathbb{R}$. Once the stationary solutions are found to be linearly unstable (i.e., $\mathrm{Im}\{\omega\} \neq 0$), then the dynamical manifestation of the corresponding instabilities is monitored through direct numerical simulations of Eq. (8). As we will see in the next section, all of the analyzed solutions are unstable, although their growth rates are so small that long propagation distances x are needed in order to observe the emergence of the pertinent instabilities.

IV. NUMERICAL RESULTS

We now present our results for the several types of coherent structures considered in our system in the self-defocusing setting (i.e., $\nu < 0$). All of them are composed of a bright soliton in the first band gap. The dark structure can be of two types. It may be a bubble, located in the first band gap and arising from the top of the second Bloch band, in which case the overall phase shift between the two endpoints of the domain is 0. Alternatively, it may be a (genuine) dark soliton, which emerges from the bottom of the second Bloch band, and, consequently, its propagation constant is found in the second

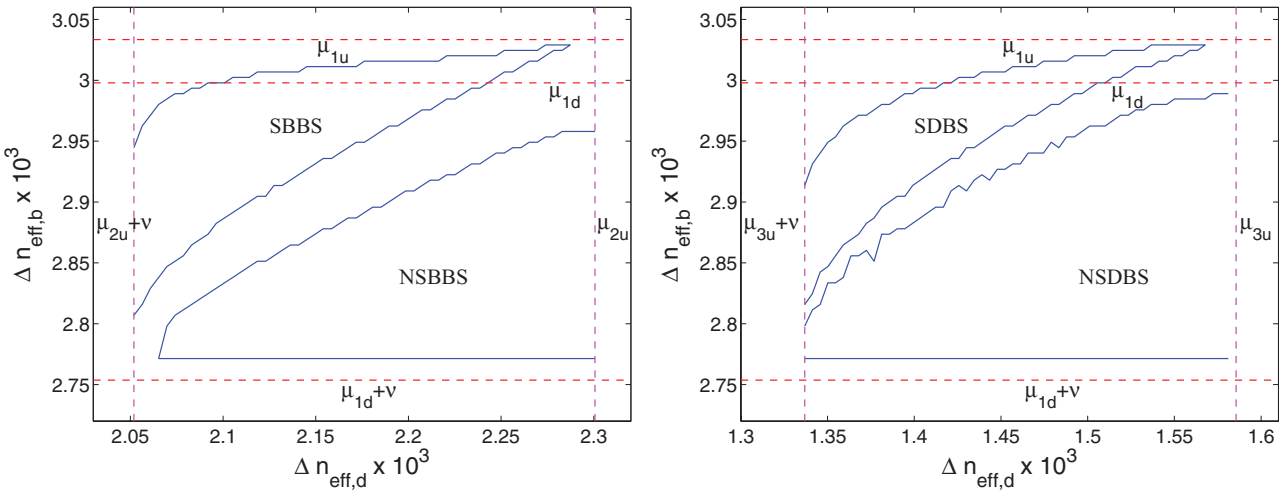

FIG. 6. (Color online) Existence range for bubble-bright (left) and dark-bright (right) solitons. Relevant endpoints of the linear spectrum (and cutoff points below which we were unable to continue the solution) are denoted by corresponding horizontal or vertical dashed lines.

band gap, and it bears a phase shift of π between the domain endpoints.

We make one more terminological distinction between the different types of waveforms that can arise. In particular, the emerging bubble (dark-bright) structures can be either symbiotic or not. In the first case, the bright soliton is unstaggered and emerges from the top of the first band (zero mode). These modes are called symbiotic because an isolated bright

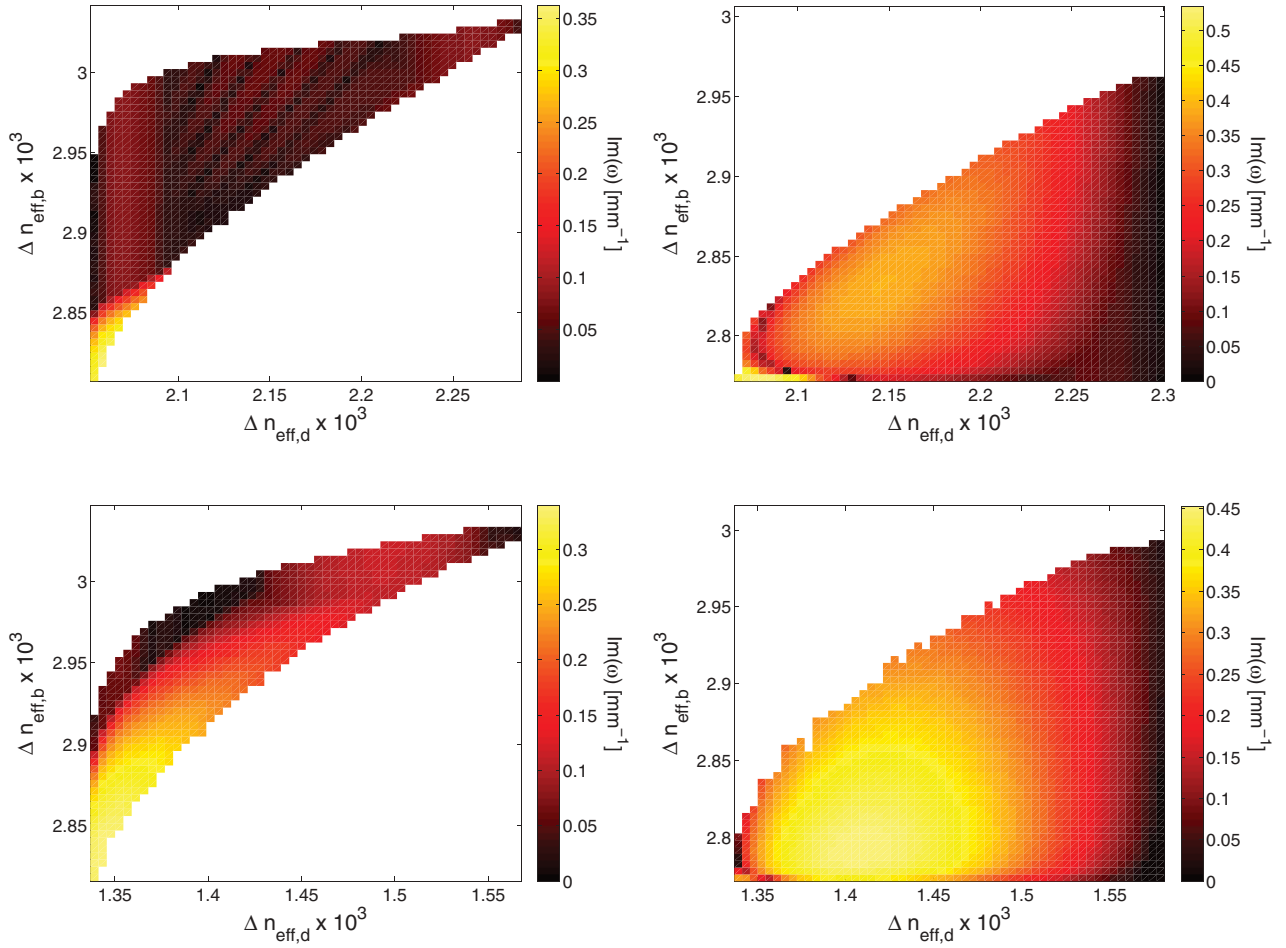

FIG. 7. (Color online) Growth rates for bubble-bright (top) and dark-bright (bottom) solitons. Left (resp. right) panels correspond to symbiotic (resp. nonsymbiotic) structures.

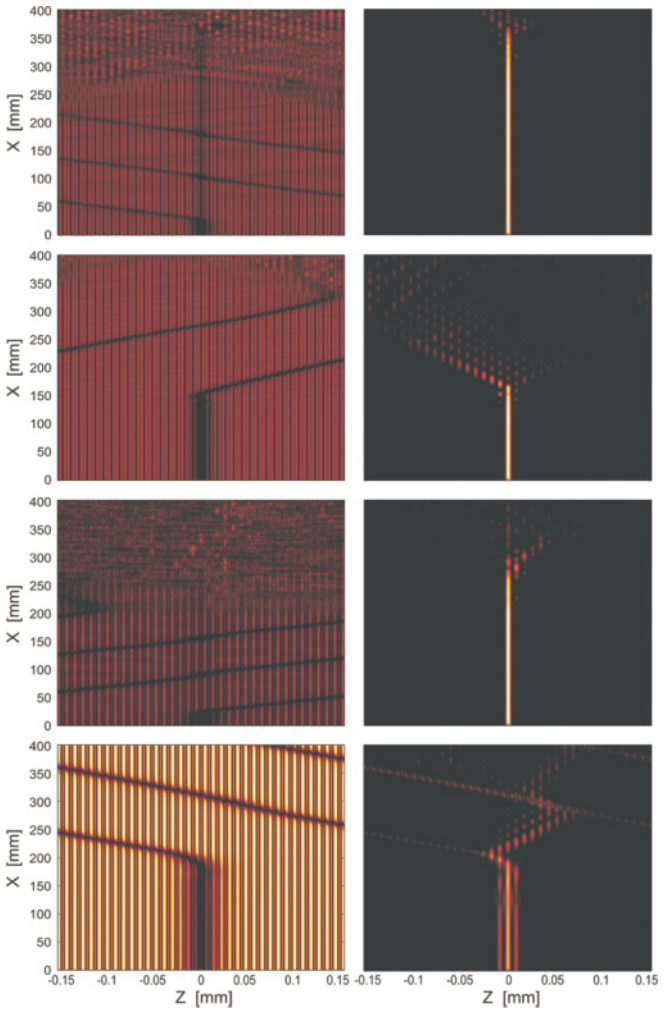

FIG. 8. (Color online) Top row: Propagation of the squared modulus of the electric field for the dark (left) and bright (right) components of a NS-BBS with $\mu_d = 0.48$ and $\mu_b = 0.635$. Second row: Propagation of the squared electric field for the dark (left) and bright (right) components of a S-BBS with $\mu_d = 0.48$ and $\mu_b = 0.67$. Third row: Propagation of the squared modulus of the electric field for the dark (left) and bright (right) components of a NS-DBS with $\mu_d = 0.32$ and $\mu_b = 0.64$. Bottom row: Propagation of the squared electric field for the dark (left) and bright (right) components of a S-DBS with $\mu_d = 0.31$ and $\mu_b = 0.66$.

component would *not* exist in this form for the relevant values of the propagation constant; it necessitates the formation of an effective potential by its dark (or bubble) counterpart in order to coexist with it. In the second (nonsymbiotic) case, the bright soliton is staggered and emerges from the bottom of the first band as a genuine gap soliton that would be sustained in the system even in the absence of the other component.

These two distinctions (dark or bubble waves for the first component, symbiotic or nonsymbiotic ones depending on the nature of the second component) give rise to four possibilities for the ensuing structures dubbed as follows: symbiotic or nonsymbiotic bubble-bright soliton (S-BBS or NS-BBS) and symbiotic or nonsymbiotic dark-bright soliton (S-DBS or NS-DBS). Among the four, it is the NS-BBS that was observed in our experimental motivation in Sec. II. Figure 5 shows prototype examples of the input field profiles for each of these four solutions.

As mentioned above, Fig. 4 shows the position of the linear Bloch bands, which are also relevant for the identification of the nonlinear localized modes that arise in the system. In particular, the first band is located in the interval $\mu_{1d} \equiv 0.6755 < \mu < 0.6833 \equiv \mu_{1u}$ [$3.00 \times 10^{-3} < n_{\rm eff} < 3.03 \times 10^{-3}$], the second one is $\mu_{2d} \equiv 0.4614 < \mu < 0.5181 \equiv \mu_{2u}$ [$2.05 \times 10^{-3} < n_{\rm eff} < 2.30 \times 10^{-3}$], and the third one at $\mu_{3d} \equiv 0.1806 < \mu < 0.3567 \equiv \mu_{3u}$ [$0.80 \times 10^{-3} < n_{\rm eff} < 1.58 \times 10^{-3}$].

Our numerical computations show that, in absence of coupling between the modes, the bright soliton can be identified in the first gap for $\mu_{1d} + \nu < \mu_b < \mu_{1d}$ (i.e., $\mu_b \in [0.6192, 0.6755]$, and ν here as well as below denotes an appropriate shift), whereas bubble-type solutions also exist for $\mu_{2u} + \nu < \mu_d < \mu_{2u}$ (i.e., $\mu_d \in [0.4618, 0.5181]$). Due to the nonlinear shift of the excited second band toward lower values of μ, the propagation constant of the bubble falls into the range of first gap of the linear band structure [43]. In turn, the dark soliton can be identified for lower values of the propagation constant, namely, for $\mu_{3u} + \nu < \mu_d < \mu_{3u}$ (i.e., $\mu_d \in [0.3004, 0.3567]$). In the case of the two coupled beam components within the waveguide array, the existence interval is narrower. Furthermore, the existence range depends qualitatively on the symbiotic or nonsymbiotic character of the soliton. More specifically, the accessible range of μ_d, for a given μ_b, is always wider for symbiotic solitons than for nonsymbiotic ones. Additionally, the existence range of symbiotic solitons is limited from above by μ_{1u}. Figure 6 depicts the existence range for dark-bright and bubble-bright symbiotic as well as nonsymbiotic solitary waves.

We have examined the linear stability of the obtained solutions, finding that the relevant waveforms are *generically* unstable in the spectral sense; i.e., we have identified an imaginary or complex eigenfrequency associated with the linearization spectrum around these profiles; however, the growth rate is typically fairly small ($\lesssim 10^{-3}$ in nondimensional units, i.e., $\lesssim 0.05$ mm^{-1} in dimensional units) and always less than 10^{-2} in nondimensional units corresponding to 0.5 mm^{-1} in dimensional ones. Consequently, instabilities appear at a sufficiently large propagation distance X (inversely proportional to the above growth rate). Figure 7 shows the growth rate dependence with $\Delta n_{\rm eff,d}$ and $\Delta n_{\rm eff,b}$ for the four analyzed structures; notice the color bar on the right indicating the magnitude of the respective growth rates. In order to test the effect of instabilities, a random perturbation of magnitude $\sim 10^{-3}$ is introduced to the input field profile. The main dynamical observed outcome is the mobility of the dark component of the soliton. This implies a breakup of the structure; however, there are two realizations thereof depending on the symbiotic or nonsymbiotic nature of the state. In the case of a nonsymbiotic solitons (i.e., for NS-BBS and for NS-DBS), the bright component remains at rest, forming a genuine bright gap soliton. On the other hand, in the symbiotic solitons, this is impossible due to the nonexistence of a bright waveform of this type. Hence, most of the bright

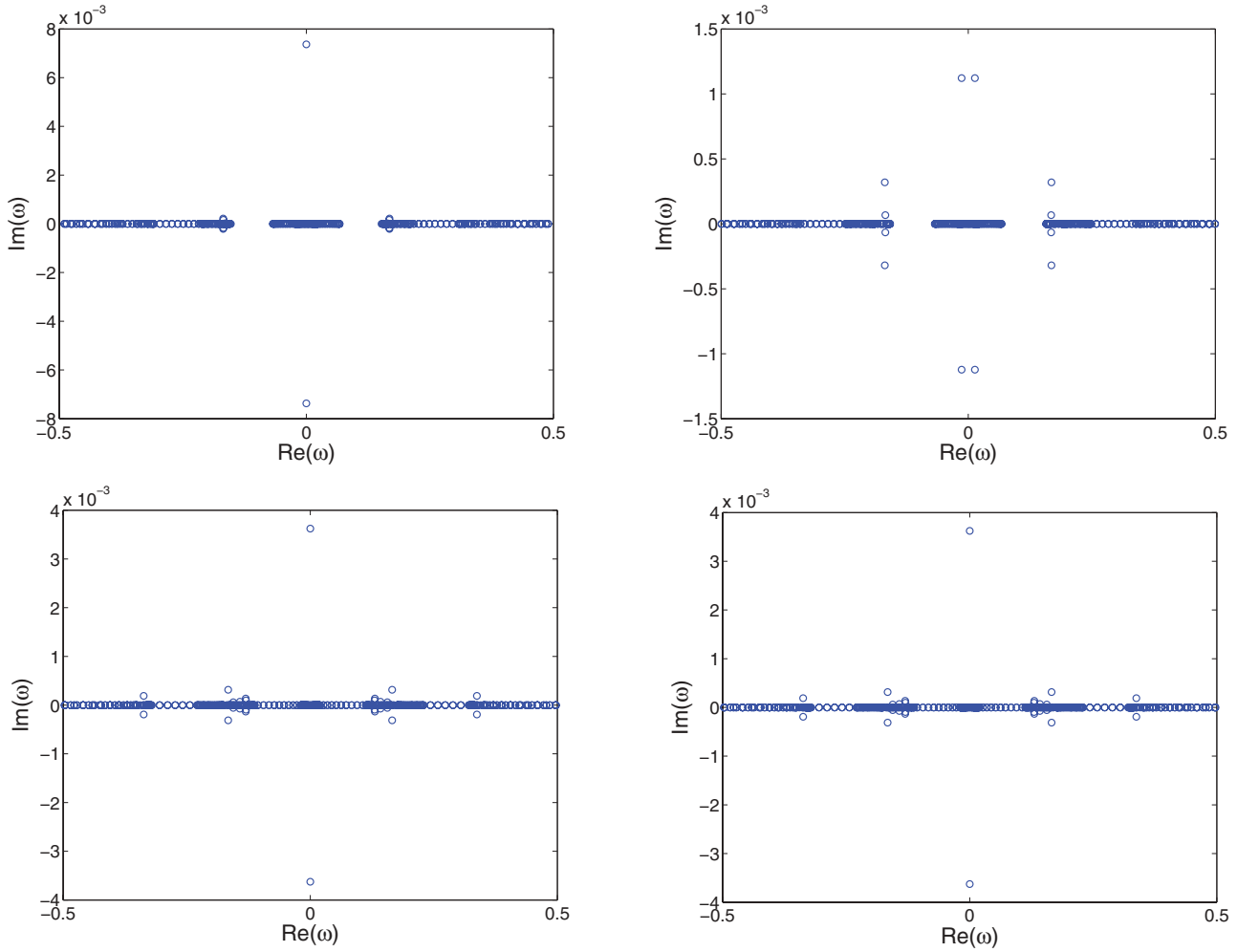

FIG. 9. (Color online) Stability panels for the solitons of Fig. 8, namely for the NS-BBS in the top left, the S-BBS in the top right, the NS-DBS of the bottom left, and S-DBS in the bottom right.

component energy moves toward the opposite direction of the dark component in the case of the bubble (i.e., for S-BBS) while part of the energy moves with the dark component. For the S-DBS, most of the energy appears to move together with the dark component. A summary of this scenario is shown in Fig. 8. To indicate the growth rates and unstable eigenmodes of the solutions dynamically followed in Fig. 8, we show in Fig. 9 their respective spectral planes. It is worth remarking that, in most cases, the instabilities are of exponential and oscillatory type, except in the case of S-BBS, where most of the instabilities are purely oscillatory. On the other hand, to connect these results with the experimental motivation of Sec. II, let us point out that for the NS-BBS considered therein the increase of the power is tantamount to a larger instability growth rate and hence the observation of the mobility of the dark component, while the bright one forms a genuine gap soliton in agreement with our numerics (top panel of Fig. 8). This repulsive effect between the two components is also evident through the blocking of the bright channel and the restoration of the bubble at the center, while the reintroduction of the interaction between the beams naturally and reversibly reinstates the repulsive bubble mobility effect.

V. CONCLUSIONS AND FUTURE CHALLENGES

In the work presented in this paper, we have considered the case of two-component dark-bright-type solitary wave states in defocusing photorefractive waveguide arrays. Motivated by experiments in $LiNbO_3$ arrays, which illustrated a bubble-type soliton state in one component coupled to a bright gap solitary wave in the second one, we delved into a theoretical examination of the different composite states that can emerge in this system. In particular, we revealed the potential for four distinct types of waves, namely, nonsymbiotic and symbiotic, dark-bright and bubble-bright ones. We numerically revealed (within a model benchmarked against the linear band structure) the persistence boundaries of such solutions. We also analyzed their linear stability, which exhibits a typically weak instability in all of them (with fairly small growth rates). This instability is so weak that it permits, apparently, the experimental observability of the states. Nevertheless, in suitable regimes even the experimental dynamics manifests the potential breakup of the composite states.

Naturally, this investigation paves the way for numerous additional studies. On the one hand, from an experimental

viewpoint it would certainly be interesting to identify the other proposed structures. On the other hand, investigating interactions of such composite structures would also offer relevant insights as was done experimentally, e.g., with simpler states in Ref. [22], or as was done numerically in Ref. [40] and in different (BEC) dark-bright contexts in Refs. [36,38]. Generalizations of such states in two-dimensional waveguide arrays with the formation of vortex-bright states [39] or of genuinely discrete variants thereof [44] would also be an exciting theme for future investigations.

ACKNOWLEDGMENTS

DK thanks the German Research Foundation (DFG, grant KI 482/11-2) for financial support of this research. PGK gratefully acknowledges support from the US-NSF through grants DMS-0806762 and CMMI-1000337 and from the Alexander von Humboldt Foundation as well as the Alexander S. Onassis Public Benefit Foundation. JC acknowledges financial support from the MICINN project FIS2008-04848.

[1] S. Aubry, Physica D **103**, 201 (1997); S. Flach and C. R. Willis, Phys. Rep. **295**, 181 (1998) ; D. Hennig and G. Tsironis, *ibid.* **307**, 333 (1999) ; P. G. Kevrekidis, K. O. Rasmussen, and A. R. Bishop, Int. J. Mod. Phys. B **15**, 2833 (2001) ; A. Gorbach and S. Flach, Phys. Rep. **467**, 1 (2008).

[2] D. N. Christodoulides, F. Lederer, and Y. Silberberg, Nature (London) **424**, 817 (2003); Yu. S. Kivshar and G. P. Agrawal, *Optical Solitons: From Fibers to Photonic Crystals* (Academic Press, San Diego, 2003).

[3] F. Lederer, G. I. Stegeman, D. N. Christodoulides, G. Assanto, M. Segev, and Y. Silberberg, Phys. Rep. **463**, 1 (2008).

[4] P. G. Kevrekidis and D. J. Frantzeskakis, Mod. Phys. Lett. B **18**, 173 (2004); V. V. Konotop and V. A. Brazhnyi, *ibid.* **18**, 627 (2004); P. G. Kevrekidis, R. Carretero-González, D. J. Frantzeskakis, and I. G. Kevrekidis, *ibid.* **18**, 1481 (2004).

[5] M. Peyrard, Nonlinearity **17**, R1 (2004).

[6] H. S. Eisenberg, Y. Silberberg, R. Morandotti, A. R. Boyd, and J. S. Aitchison, Phys. Rev. Lett. **81**, 3383 (1998).

[7] R. Morandotti, U. Peschel, J. S. Aitchison, H. S. Eisenberg, and Y. Silberberg, Phys. Rev. Lett. **83**, 2726 (1999).

[8] D. Mandelik, R. Morandotti, J. S. Aitchison, and Y. Silberberg, Phys. Rev. Lett. **92**, 093904 (2004).

[9] J. Meier, G. I. Stegeman, D. N. Christodoulides, Y. Silberberg, R. Morandotti, H. Yang, G. Salamo, M. Sorel, and J. S. Aitchison, Phys. Rev. Lett. **92**, 163902 (2004).

[10] J. Meier, J. Hudock, D. N. Christodoulides, G. Stegeman, Y. Silberberg, R. Morandotti, and J. S. Aitchison, Phys. Rev. Lett. **91**, 143907 (2003).

[11] S. Suntsov, K. G. Makris, D. N. Christodoulides, G. I. Stegeman, A. Haché, R. Morandotti, H. Yang, G. Salamo, and M. Sorel, Phys. Rev. Lett. **96**, 063901 (2006).

[12] N. K. Efremidis, S. Sears, D. N. Christodoulides, J. W. Fleischer, and M. Segev, Phys. Rev. E **66**, 046602 (2002).

[13] J. W. Fleischer, M. Segev, N. K. Efremidis, and D. N. Christodoulides, Nature (London) **422**, 147 (2003).

[14] H. Martin, E. D. Eugenieva, Z. Chen, and D. N. Christodoulides, Phys. Rev. Lett. **92**, 123902 (2004); J. W. Fleischer, T. Carmon, M. Segev, N. K. Efremidis, and D. N. Christodoulides, *ibid.* **90**, 023902 (2003).

[15] J. Yang, I. Makasyuk, A. Bezryadina, and Z. Chen, Opt. Lett. **29**, 1662 (2004).

[16] J. Yang, I. Makasyuk, P. G. Kevrekidis, H. Martin, B. A. Malomed, D. J. Frantzeskakis, and Z. Chen, Phys. Rev. Lett. **94**, 113902 (2005).

[17] Y. V. Kartashov, V. A. Vysloukh, and L. Torner, Phys. Rev. Lett. **93**, 093904 (2004); X. Wang, Z. Chen, and P. G. Kevrekidis, *ibid.* **96**, 083904 (2006).

[18] D. N. Neshev, T. J. Alexander, E. A. Ostrovskaya, Yu. S. Kivshar, H. Martin, I. Makasyuk, and Z. Chen, Phys. Rev. Lett. **92**, 123903 (2004).

[19] J. W. Fleischer, G. Bartal, O. Cohen, O. Manela, M. Segev, J. Hudock, and D. N. Christodoulides, Phys. Rev. Lett. **92**, 123904 (2004).

[20] G. Bartal, O. Manela, O. Cohen, J. W. Fleischer, and M. Segev, Phys. Rev. Lett. **95**, 053904 (2005).

[21] C. E. Rüter, J. Wisniewski, M. Stepic, and D. Kip, Opt. Express **15**, 6324 (2007).

[22] M. Stepić, E. Smirnov, C. E. Rüter, L. Prönneke, D. Kip, and V. Shandarov, Phys. Rev. E **74**, 046614 (2006).

[23] E. Smirnov, C. E. Rüter, M. Stepić, D. Kip, and V. Shandarov, Phys. Rev. E **74**, 065601 (2006).

[24] D. Kip, C. E. Rüter, R. Dong, Z. Wang, and J. Xu, Opt. Lett. **33**, 2056 (2008).

[25] R. Dong, C. E. Rüter, D. Song, J. Xu, and D. Kip, Opt. Express **18**, 27493 (2010).

[26] K. Shandarova, C. E. Rüter, D. Kip, K. G. Makris, D. N. Christodoulides, O. Peleg, and M. Segev, Phys. Rev. Lett. **102**, 123905 (2009).

[27] Z. Chen, A. Bezryadina, I. Makasyuk, and J. Yang, Opt. Lett. **29**, 1656 (2004).

[28] R. A. Vicencio, E. Smirnov, C. E. Rüter, D. Kip, and M. Stepić, Phys. Rev. A **76**, 033816 (2007).

[29] Z. Chen, M. Segev, T. H. Coskun, D. N. Christodoulides, Yu. S. Kivshar, and V. V. Afanasjev, Opt. Lett. **21**, 1821 (1996).

[30] E. A. Ostrovskaya, Yu. S. Kivshar, Z. Chen, and M. Segev, Opt. Lett. **24**, 327 (1999).

[31] T. Busch and J. R. Anglin, Phys. Rev. Lett. **87**, 010401 (2001).

[32] H. E. Nistazakis, D. J. Frantzeskakis, P. G. Kevrekidis, B. A. Malomed, and R. Carretero-González, Phys. Rev. A **77**, 033612 (2008).

[33] C. Becker, S. Stellmer, P. Soltan-Panahi, S. Dörscher, M. Baumert, E.-M. Richter, J. Kronjäger, K. Bongs, and K. Sengstock, Nature Phys. **4**, 496 (2008).

[34] C. Hamner, J. J. Chang, P. Engels, and M. A. Hoefer, Phys. Rev. Lett. **106**, 065302 (2011).

[35] M. A. Hoefer, C. Hamner, J. J. Chang, and P. Engels, e-print arXiv:1007.4947v1 [http://arxiv.org/abs/1007.4947].

[36] S. Middelkamp, J. J. Chang, C. Hamner, R. Carretero-González, P. G. Kevrekidis, V. Achilleos, D. J. Frantzeskakis, P. Schmelcher, and P. Engels, Phys. Lett. A **375**, 642 (2011).
[37] S. Rajendran, P. Muruganandam, and M. Lakshmanan, J. Phys. B **42**, 145307 (2009).
[38] C. Yin, N. G. Berloff, V. M. Pérez-García, D. Novoa, A. V. Carpentier, and H. Michinel, Phys. Rev. A **83**, 051605(R) (2011).
[39] K. J. H. Law, P. G. Kevrekidis, and L. S. Tuckerman, Phys. Rev. Lett. **105**, 160405 (2010).
[40] A. Álvarez, J. Cuevas, F. R. Romero, and P. G. Kevrekidis, Physica D **240**, 767 (2011).
[41] D. Kip, Appl. Phys. B **67**, 131 (1998).
[42] C. E. Rüter, J. Wisniewski, and D. Kip, Opt. Lett. **31**, 2768 (2006).
[43] C. E. Rüter and D. Kip, Phys. Rev. A **77**, 013818 (2008).
[44] J. Cuevas, Q. E. Hoq, H. Susanto, and P. G. Kevrekidis, Physica D **238**, 2216 (2009).